communications biology

Article

https://doi.org/10.1038/s42003-024-06827-w

The secretory protein COA1 enables *Metarhizium robertsii* to evade insect immune recognition during cuticle penetration

Check for updates

Qiangqiang Zhang[1,2], Xuanlian Wei[3], Weiguo Fang[4], Xuenian Huang[1,2] & Xing Zhang[3]

The interplay between the insect immune system and entomopathogenic fungi during cuticle penetration is not yet fully understood. Here, we show that a secretory protein COA1 (coat of appressorium 1) from *Metarhizium robertsii*, an entomopathogenic fungus causing diseases in a wide range of insects, is required to avoid host immune recognition during cuticle penetration. COA1 is highly expressed on the cuticle and translocated to the cell surface, where it directly binds with and masks carbohydrates of the fungal cell wall to avoid provoking the host's intense immune response. Deletion of *Coa1* results in a robust immune response, leading to a reduction in bacterial load in both the gut and hemocoel and ultimately attenuating fungal virulence. Our work reveals a novel cell surface protein indispensable for fungal pathogenicity via masking cell wall carbohydrates to avert a hypersensitive response from the host.

Unlike viruses and bacteria that need *per os* infections, entomopathogenic fungi such as *Beauveria and Metarhizium* species are capable of breaching the cuticle of a wide range of insect pests, and are widely used as biological insecticides and models for studying fungal pathogenesis in insects[1–3]. Infection begins with spore adherence to insect cuticles, and spores germinate to produce the infection structure appressorium to penetrate the cuticle. Once entering the hemocoel, the fungi dimorphically change from filamentous development to hyphal bodies (yeast-like blastopores) and produce toxins to kill insects[4].

During a long period of co-evolution, insect pathogenic fungi have evolved diverse strategies to evade or breach the host defense systems. During cuticle penetration, fungi secrete an array of cytochrome P450 enzymes, lipases, and dehydrogenases to help detoxify antifungal compounds produced by the host[5–8]. It has been observed that defensive microbiomes on insect cuticles can hamper the invasion of entomopathogenic fungi[9,10]. To overcome this, *Beauveria bassiana* or *Metarhizium robertsii* secretes fungal defensin BbAMP1 or helvolic acid to suppress cuticular microbes and facilitate fungal infection[9,10].

When a pathogenic fungus breaches epithelial barriers and enters the hemocoel, the host launches an attack to eliminate foreign intruders via cellular and humoral responses shared in part with higher organisms[11], i.e., phagocytosis, encapsulation, melanization reaction, or antimicrobial peptides (AMPs) secreted by fat bodies[12]. Many mechanisms have been discovered for fungi to circumvent or subvert host immune attacks during hemocoel colonization. For instance, fungi can remodel the cell wall architecture or express the collagenous protein MCL1 to mask antigenic cell wall structural components[13,14], or express toxins like destruxin or oosporein to bring down the host's immune response[15,16]. Changing the protease expression profile[17–19], or expressing the cell surface protein BbLac2[20], can inhibit insect phenoloxidase (PO) activity. The endo-β-1,3-glucanase BbEng1 can modify hyphal bodies'carbohydrate epitopes, facilitating *B. bassiana* to evade host immune attack[21].

The fungal cell wall, mainly composed of glucans, chitin, and other polysaccharides linked to proteins and lipids[22], is an essential structure for protecting fungi from environmental stress. Simultaneously, it is a prime structure for host recognition[23,24]. For a long time, insects were thought only to identify and fight back systemically after the pathogenic fungi reached the epidermis layer and entered the hemocoel. However, a recent study has shown that locusts are capable of detecting β-1,3-glucan of the *M. acridum* cell wall before fungal cuticular penetration occurs, triggering the release of antimicrobial peptides (AMPs)[25]. The effect of this immune response on fungal pathogenicity is unknown. Several studies have reported that topical

[1]Shandong Provincial Key Laboratory of Synthetic Biology, Qingdao Institute of Bioenergy and Bioprocess Technology, Chinese Academy of Sciences, Qingdao, 266101 Shandong, China. [2]Qingdao New Energy Shandong Laboratory, Qingdao, 266101, China. [3]Department of Pathogenic Biology, School of Basic Medicine, Qingdao University, Qingdao, 266101 Shandong, China. [4]MOE Key Laboratory of Biosystems Homeostasis & Protection, Institute of Microbiology, College of Life Science, Zhejiang University, Hangzhou, China. e-mail: zhangxing_hubu@163.com

infection with entomopathogenic fungi leads to hosts' gut microbiome dysbiosis[26,27]. As hosts can respond to fungi on the cuticle, it prompts further investigation into how this host-pathogen interaction during cuticle penetration influences the insect immune status and insect microbiome. Furthermore, the exposure of more antigenic cell wall components due to conidia germination and appressorium formation on the cuticle[28] raises the question of whether a protective coat exists to avoid provoking an intense host immune response.

In this study, we report that a highly expressed secreted protein COA1 can protect fungi from host recognition and effectively avoid intense immune responses in the hemocoel and gut during the cuticle penetration stage. COA1 can bind directly with immunogenic cell wall constituents. The disruption of *Coa1* leads to an upsurge in immune effector expression and a substantial decrease in bacteria titers in the insect's blood and gut. The discovery of the new coat protein COA1 sheds light on the mechanism entomopathogenic fungi employ to evade immune recognition during cuticle penetration, expanding our knowledge of host-fungi immune interactions.

Results

Identification of virulence-related protein COA1

Our previous ChIP-Seq and RNA-Seq data suggested that virulence-related transcription factor COH2 could directly bind to MAA_08843 (named as *Coa1*, as it functions as a coat protein of appressorium) promoter and positively regulate its expression[19]. To confirm the ChIP-Seq data, we performed a ChIP-qPCR analysis using primers to cover the COH2 DNA binding motif in the *Coa1* promoter. The results demonstrated an 18.9-fold higher fold enrichment in the aforementioned region in the WT-COH2-FLAG strain compared to the WT-FLAG strain, as shown in Fig. 1a. During penetrating the cuticle, qRT-PCR revealed a 63-fold decrease in *Coa1* expression levels in Δ*Coh2* (Fig. 1b).

According to qRT-PCR analysis, the *Coa1* transcript was highly expressed on the real insect cuticle and under mimic cuticle conditions, i.e., the hydrophobic surface in nutrient-deprived conditions. During saprophytic growth (including PDB, liquid medium; PDA, solid medium; conidia) and hemocoel colonization, *Coa1* expression showed no significant variation (Fig. 1c). To reflect the realistic expression pattern of *Coa1*, we constructed the *WT-PCoa1-GFP* strain, in which the *Coa1* promoter drove the *gfp* gene in the wild type, and the GFP fluorescent intensity is proportional to the *Coa1* expression level. In line with the qRT-PCR results, fungi on the *Galleria mellonella* cuticle and under mimic cuticle condition showed a higher GFP fluorescent intensity than those in real hemocoel and saprophytic growth conditions (Fig. 1d). A time course analysis of *Coa1* expression revealed a 28.6-fold increase in *Coa1* after eight hours of inoculation on aseptic and isolated *G. mellonella* cuticle (conidia began to germinate), escalating further to 697-fold at 16 h (when appressorium could be detected) and maintained at high levels up to 30 h (appressorium maturation), 36 h and 48 h (cuticle penetration was complete) compared to 0 h (Fig. 1e). The GFP signal of the *WT-PCoa1-GFP* strain at various stages of *M. robertsii* infection also indicates high expression of *Coa1* throughout the entire cuticle penetration process. As depicted in Fig. 1f, strong GFP signals were observed in the conidia, germinated hyphae, mature appressorium, and the penetration hyphae reaching the endocuticle.

To explore the biological function of *Coa1*, we performed deletion and complementation of *Coa1* in *M. robertsii* (Supplementary Fig. 1). No significant differences were found between the colony morphology, growth, and conidial yield of *ΔCoa1* and the WT strain on several media (Supplementary Fig. 2a–c). No detectable differences were observed between *Coa1* mutant, complementation, and WT strains when the fungi confronted oxidants (H_2O_2 and menadione), osmotic agent (sorbitol), and cell wall-disturbing agents (CFW and Congo red) (Supplementary Fig. 2c). However, the *Coa1* mutant displayed increased sensitivity to high salt stress (Supplementary Fig. 2d). According to the qRT-PCR analysis, the expression of *Coa1* was not induced by high salt stress (Supplementary Fig. 2e).

Fungal virulence was assessed using *G. mellonella* larvae. Topical infection was employed to determine the median lethal time (LT_{50}) of the mutant *ΔCoa1* (12.4 ± 0.5 days), which was found to be 1.7-fold longer than that of the WT strain (7.3 ± 0.3 days) ($P < 0.001$). The complemented strain *C-ΔCoa1* and the WT strain showed no significant difference ($P > 0.05$) (Fig. 1g). Further direct injection to bypass the insect cuticles was conducted, and the results indicated no significant difference between *ΔCoa1*, WT, and *C-ΔCoa1* (Supplementary Fig. 3a). On the hydrophobic surfaces, no difference in appressorium formation rate and lipid droplet (LD) storage, as indicated by fluorescent staining of LDs, was found between the *ΔCoa1* and WT strains (Supplementary Fig. 3b, c). The *Coa1* mutant and WT strains exhibited similar abilities to penetrate the cuticle of *G. mellonella* (Supplementary Fig. 3d). These results indicated that COA1 was indispensable for fungal pathogenicity but not involved in appressorium formation.

COA1 localizes on the fungal cell surface during penetrating insect cuticles

Coa1 putatively encodes a 69 aa protein via a 210 bp open reading frame. Protein sequence analysis using SignalP-6.0 (https://services.healthtech.dtu.dk/services/SignalP-6.0/) revealed a Sec/SPI type signal peptide at the N-terminus with a high probability of 0.9996. TMHMM-2.0 (https://services.healthtech.dtu.dk/services/TMHMM-2.0/) indicated no transmembrane helices, suggesting that COA1 is a secreted small protein. To evaluate protein subcellular localization, we introduced the gene cassettes *Coa1-gfp* and *gfp* under the native *Coa1* promoter into the *Coa1* mutant to obtain *ΔCoa1-PCoa1-Coa1-GFP* and *ΔCoa1-PCoa1 -GFP* strains. The correct fusion protein expression was confirmed by Western blot analysis (Fig. 2a). GFP signals were observed by fluorescence microscopy 48 h post inoculation (hpi) of*ΔCoa1-PCoa1-Coa1-GFP* and *ΔCoa1-PCoa1 -GFP* strains on alive *G. mellonella* larvae. The result indicated that the COA1::GFP localized on the cell wall surface (Fig. 2b). To further corroborate this result, a fluorescent dye was used to confirm the localization of COA1. After inoculation on hydrophobic surfaces under nutrient starvation conditions, which mimic the real insect cuticle condition, COA1 was translocated to the cell surface, as confirmed by the fluorescent dye CFW (Fig. 2c).

COA1 binds to carbohydrates present on the fungal cell wall

We used fluorescently labeled lectins and antibodies for the specific staining and quantitative analysis of WT, *ΔCoa1*, and *C-ΔCoa1* cell wall carbohydrates, to investigate whether COA1 influences cell wall constituents. These included probing with Concanavalin A (ConA), wheat germ agglutinin (WGA), peanut agglutinin (PNA), Helix pomatia agglutinin (HPA), and β-1,3-glucan antibody. During appressorium formation, there was an apparent rise in fluorescence intensity of ConA, HPA, WGA, and β-1,3-glucan in *ΔCoa1* compared to the WT and *C-ΔCoa1* ($P < 0.0001$) (Fig. 3). However, no discernible variation between them for PNA ($P > 0.05$) was observed (Supplementary Fig. 4a). During saprophytic growth on the PDB media, no noticeable difference in fluorescence intensity was found between WT, *ΔCoa*1, and *C-ΔCoa1* (Supplementary Fig. 4b).

As shown in Fig. 3, there is an increased fluorescence intensity of chitin (determined by staining with HPA and WGA), mannan (determined by staining with ConA), and β-1,3-glucan in *ΔCoa*1, which suggests that COA1 may affect these carbohydrate contents. However, carbohydrate content analysis showed chitin, mannan, and β-1,3-glucan were not significantly different between WT, *ΔCoa*1, and *C-ΔCoa*1 (Supplementary Fig. 5a–c). To investigate whether COA1 affected the exposure of the carbohydrates on the surface of fungi, we examined the ability of COA1 to bind with chitin, mannan, and β-1,3-glucan. The recombinant protein COA1 was expressed in *Escherichia coli* and purified for the binding assay (Fig. 4a, b). The results revealed that COA1 could directly bind with mannan, chitin, and β-1,3-glucan (Fig. 4c). Molecular docking analysis was performed to evaluate the affinity of COA1 for carbohydrates. Using Autodock Vina v.1.2.2, we determined the binding pose and interaction of β-1,3-glucan trimer (linked by beta-1,3 glycosidic bond) or D-GlcNAc trimer (linked by beta-1,4

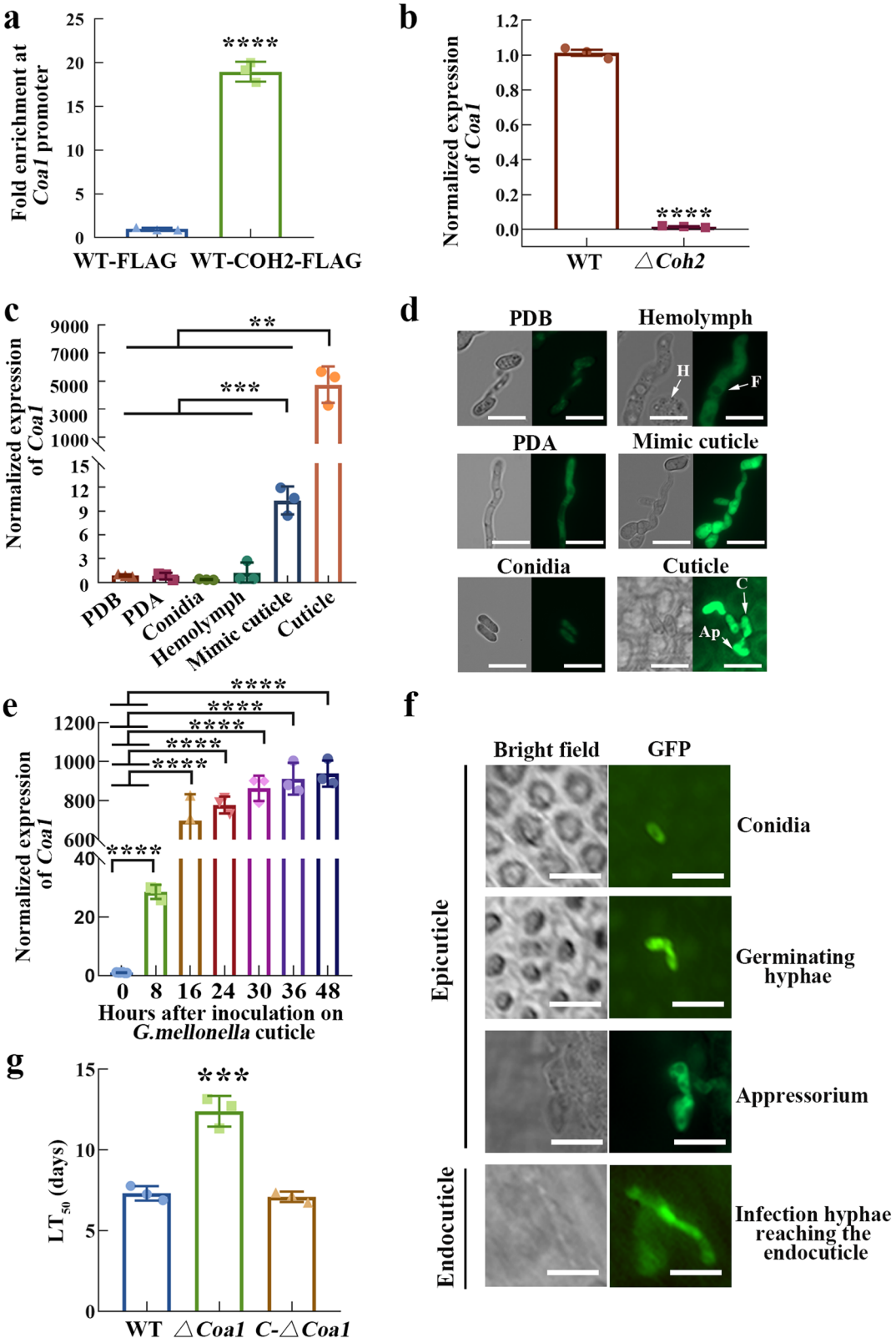

glycosidic bond) with COA1 protein (Fig. 4d). The binding energy for β-1,3-glucan and COA1 was −4.864 kcal/mol, and −4.821 kcal/mol for D-GlcNAc and COA1. There were six visible hydrogen bonds for COA1 and β-1,3-glucan interaction and seven for D-GlcNAc and COA1. The molecular docking of mannan and COA1 was not simulated in this study because mannan is exclusively found in fungi as a glycoconjugate and is not present as an unconjugated oligosaccharide[29], and we could not find a proper compound from the PubChem database. To further validate that COA1 could bind to the fungal cell wall, COA1::His or control proteins were incubated with the appressorium cultivated on the hydrophobic dishes. The observed OD450 values also indicated that COA1 could bind to carbohydrates on the fungal cell wall (Fig. 4e).

Fig. 1 | Regulation and expression of *Coa1*. **a** ChIP-qPCR analysis indicates that COH2 directly binds to the *Coa1* promoter. WT-COH2-FLAG is a strain expressing the fusion protein COH2::FLAG. **b** qRT-PCR analysis of *Coa1* expression in the *ΔCoh2* mutant compared to the WT during penetrating cuticle. (****$P < 0.0001$, $n = 3$, two-tailed Student's t test). **c** *Coa1* expression during saprotrophic growth (PDB, PDA, Conidia), penetrating cuticle (Cuticle, Mimic cuticle), and colonizing hemocoel (Hemolymph) (**$P < 0.01$, ***$P < 0.001$, $n = 3$, two-tailed Student's t test). PDB, 10^8 conidia of WT strain cultured in 100 mL of PDB media for 36 h; PDA, conidia inoculated on a PDA plate for 3 days; Conidia: collected from 14 day-old-PDA plates; Cuticle: conidia inoculated onto the cuticle of *G. mellonella* for 30 h; Mimic cuticle: conidia inoculated onto the hydrophobic Petri dish containing 0.0125% yeast extract for 16 h; Hemolymph, 10^5 conidia were inoculated into 250 μL of *G. mellonella* larvae hemolymph mixture for 36 h. **d** GFP signal in the fungal cells in different conditions described in **c**. The *Coa1* promoter drives *gfp*. Scale bar: 10 μm. F fungal cells, H hemocyte, C conidia, Ap appressorium. **e** Relative expression of *Coa1* after being inoculated on the isolated and sterilized cuticle for different hours. The *Coa1* expression at 0 h was set as 1. $n = 3$, ****$P < 0.0001$, two-tailed Student's t test. **f** GFP signals were observed in the fungal cells of the strain *WT-PCoa1-GFP* at various developmental stages of *M. robertsii* infection. The detection of GFP in the endocuticle indicates the completion of the cuticle penetration process. Scale bar: 10 μm. **g** LT_{50} values after topical infection. The experiments were conducted three times, with 40 insects in each repetition. ***$P < 0.001$, Tukey's test in one-way ANOVA. The data is presented as the mean ± SD.

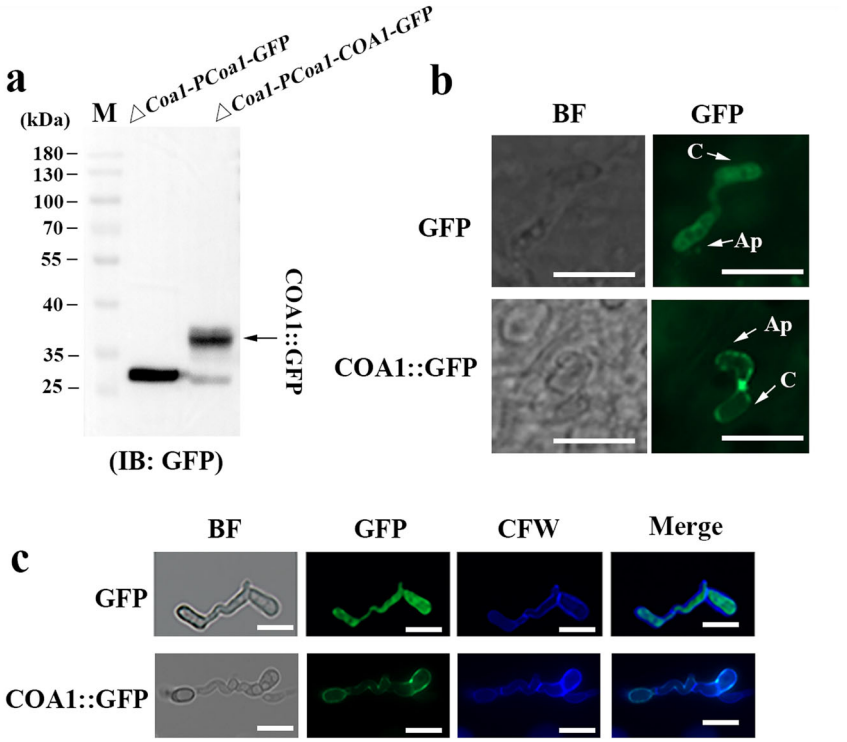

Fig. 2 | Subcellular localization of COA1. **a** Western blot was used to verify the COA1::GFP fusion protein construct. The protein band indicated by the black arrow is COA1::GFP fusion protein. **b** Localization of COA1 on the alive *G. mellonella* larvae cuticle. After inoculating conidia on the *G. mellonella* for 48 h, the insects and fungal culture were frozen at −80 °C. After dissecting the insect to obtain the cuticle, the GFP was observed under a fluorescent microscopy. Ap appressorium, C conidia. Scale bar: 10 μm. **c** COA1 is transported to the cell surface during appressorium formation on the hydrophobic surfaces. After being induced to form appressorium on the hydrophobic plastic dishes for 16 h, the samples were stained with Calcofluor White (CFW, stain chitin of cell wall). The upper panel shows cells with free GFP (control), and the lower panel shows images with COA1::GFP fusion protein. Scale bars represent 10 μm. Merge, merge of CFW and GFP images.

COA1 is essential for fungi to avoid provoking intense immune responses

Insects can recognize the fungal cell wall components and subsequently activate immune responses. The fat body and epidermal cells can synthesize antimicrobial peptides (AMPs) against microbial attacks. We thus explored the effect of COA1 on the fungal's ability to evade host innate immune responses. We examined the expression of seven AMPs in the insect hemolymph, identified in previous work[30], after topical infection with different strains at 12, 24, 48, 72, and 96 h. We tracked the fungal developmental processes after inoculation on live *G. mellonella* larvae. Conidial germination occurred at 24 h, with appressoria visible at 48 h. By 72 hpi, fungi could be observed in the endocuticle and epidermis, indicating that cuticle penetration was complete (Supplementary Fig. 6a). The expression level of antimicrobial peptides in mock control (insects treated with 0.01% Triton X-100) at 24 h was set as 1. All seven genes in the fat bodies showed slight upregulation at 12 h and downregulation at 24 h in the mock control. The reason might be that the inoculation method temporarily perturbed the insect immune system's homeostasis. Antimicrobial peptide expression levels in the mock, WT, and *ΔCoa1* were similar at 12 h (Fig. 5a). After topical infection with WT, all the tested AMPs except for *moricin*, were significantly upregulated at 24 and 48 h compared with the mock control. Different AMP expression trends over time was observed. Specifically, *gallerimycin*, *6tox*, and *GMpro1* peaked at 24 h, whereas *cecropin A* attained peak levels at 48 h (Fig. 5a). Notably, unlike the WT, the *Coa1* mutant provoked a robust humoral immune response. All the tested AMP expression levels, except for *GMpro1* and *galiomicin*, showed a significant difference between the WT and *ΔCoa1* at 24 and 48 h (Fig. 5a). Importantly, all the expression levels of AMPs declined to the base level by 96 h (Fig. 5a). Expression of AMPs in epithelial cells was also explored. All the tested AMPs, except for *moricin*, were significantly upregulated at 24 and 48 h after topical infection with WT spores compared with the mock control (Supplementary Table 1). However, no notable distinction was observed between the WT and *ΔCoa1* ($P > 0.05$) (Supplementary Table 1).

AMPs in the insect gut are essential for maintaining gut microbiota homeostasis. Besides the AMPs, we also analyzed the expression of two other immune effectors in the gut: dual oxidase (duox), which catalyzes hydrogen peroxide production, and lysozyme, which destroys the cell wall of gram-positive bacteria[31]. Expression of *GMpro1*, *gloverin*, *6tox*, and *duox* was not significantly different between the WT and mock control (Fig. 5b). At 24 and 48 h, the expression of *gallerimycin, galiomicin*, *cecropin A*, and *lysozyme* was comparable to the mock control, but at 72 h, they were upregulated by 18-, 3.8-, 8.2-, and 7.0-fold change, respectively. *Moricin* was downregulated 21.3-fold at 48 h, but there was no difference at 24 and 72 h compared with the mock control (Fig. 5b). All detected genes,

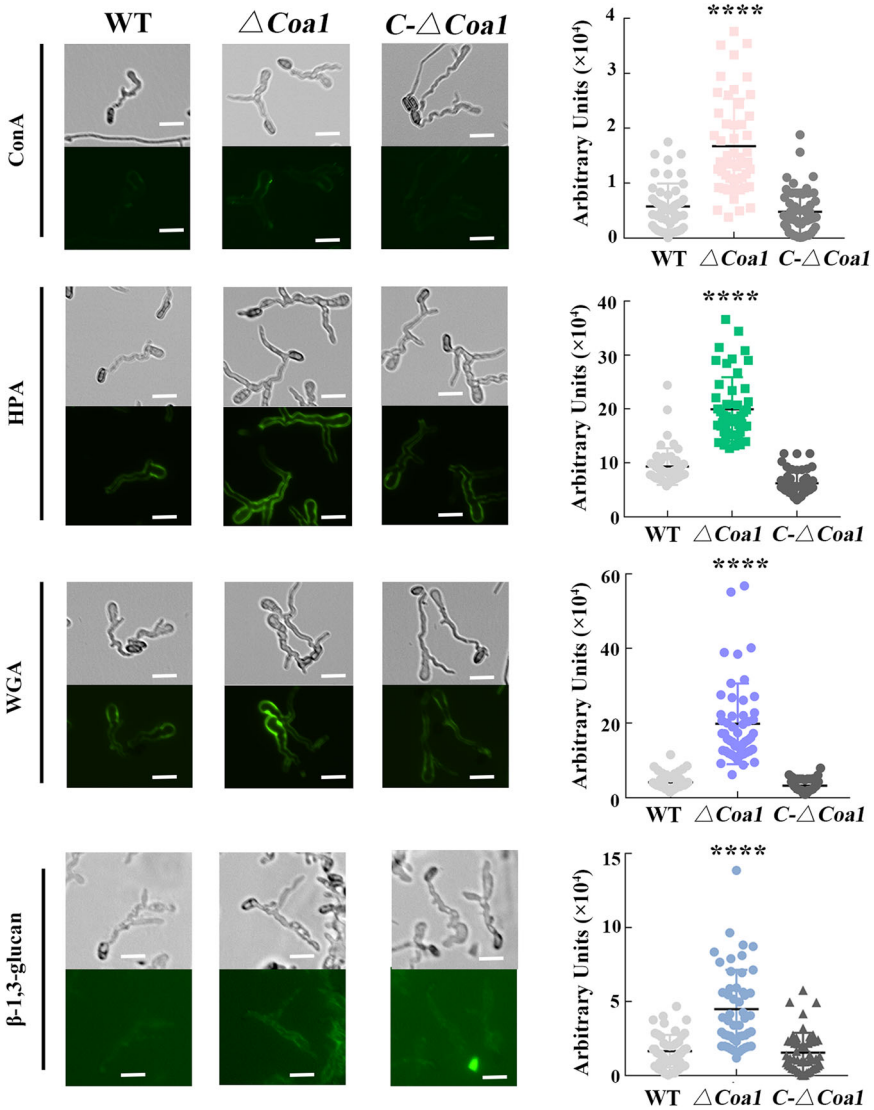

Fig. 3 | Lectin staining was used to compare the exposure of different carbohydrates on the appressorium. The WT, *ΔCoa1*, and *C-ΔCoa1* spores were inoculated in a low nutrient medium (0.0125% yeast extract) on the hydrophobic dishes for 16 h and then stained by different lectins. ConA (Concanavalin A) was used to stain mannan. HPA (Helix pomatia agglutinin) and WGA (wheat germ agglutinin) were used to stain chitin. The β-1,3-glucan was detected using a β-1,3-glucan antibody with a FITC-conjugated secondary antibody. Scale bar, 10 μm. The bar graphs in the right panel summarize the mean fluorescence intensity averaged from fifty cells in each strain. The statistical analyses were performed using Tukey's test in one-way ANOVA ($n = 50$, **** indicates $P < 0.0001$). The data is presented as the mean ± SD.

except for *gloverin*, *6tox*, and *duox*, were significantly upregulated in the *ΔCoa1*-infected larvae gut compared with the mock and WT at 24 or 48 hpi (Fig. 5b). We also analyzed the phenoloxidase activity in the hemolymph after topical infection with different strains. However, no significant difference was found in the mock, WT, and *ΔCoa1* at 24, 48, and 72 h (Supplementary Fig. 6b).

To further verify the carbohydrate-binding and immune-escape capacity of COA1, we injected a mixture of purified COA1::His or crude extract of *E. coli* with empty vector (pET-28a, control) protein and different carbohydrates into the insect hemocoel. Ten minutes later, insects injected with the control protein and carbohydrates showed apparent melanization and high phenoloxidase activity. No such intense immunoreactivity was observed in insects injected with the COA1::His-carbohydrates mixture (Fig. 5c). Following the injection of the insect with the protein, and subsequent exposure to carbohydrates with a five-minute intermission, the COA1::His protein exhibited its ability to inhibit the melanization reaction (Supplementary Fig. 6c). A slight melanization was observed in the abdomens of insects that were initially injected with carbohydrates, followed by the COA1::His protein. Notably, the PO activity in these insects was lower than in those injected with the control protein, as shown in Supplementary Fig. 6d. The expression levels of AMPs upregulated after being injected with a protein-carbohydrate mixture compared with the mock. However, there was no notable difference between the control-carbohydrates and COA1::His-carbohydrates mixture treatment (Supplementary Fig. 6e, f, g).

Fungal infection leads to gut microbiome dysbiosis

As shown in Fig. 5b, topical infection with entomopathogenic fungi altered the expression of gut immune effectors, potentially leading to changes in the gut microbiome. After topical infection with different strains, the insects were dissected to individually obtain the gut and determine the culturable bacteria load by plating. The results showed that *ΔCoa1* significantly reduced the gut bacteria load compared to the mock and WT-infected insects (Fig. 6a). The total gut bacteria DNA was extracted individually for quantitative PCR (qPCR) using universal 16S rRNA primers, validating the decrease in gut bacterial load at 48 and 72 h after topical infection with *ΔCoa1*(Fig. 6b).

Although topical infection with the WT strain did not affect the gut bacteria load, the plating assay suggested alterations in bacterial composition (Fig. 6a). We next performed gut microbiome analysis on the *G. mellonella* after topical infection with different strains at 48 h. The results showed striking relative bacterial abundance differences among the strains in the gut at both the phylum and genus levels (Fig. 6c, d). In the uninfected insects, the microbiota was composed mainly of the *Firmicutes* and *Proteobacteria* phylum. In contrast, the single phylum *Firmicutes* was dominated in the WT or *ΔCoa1*-infected insects (Fig. 6c). At the genus level, *Enterococcus* increased; at the same time *Klebsiella* and *Proteus*

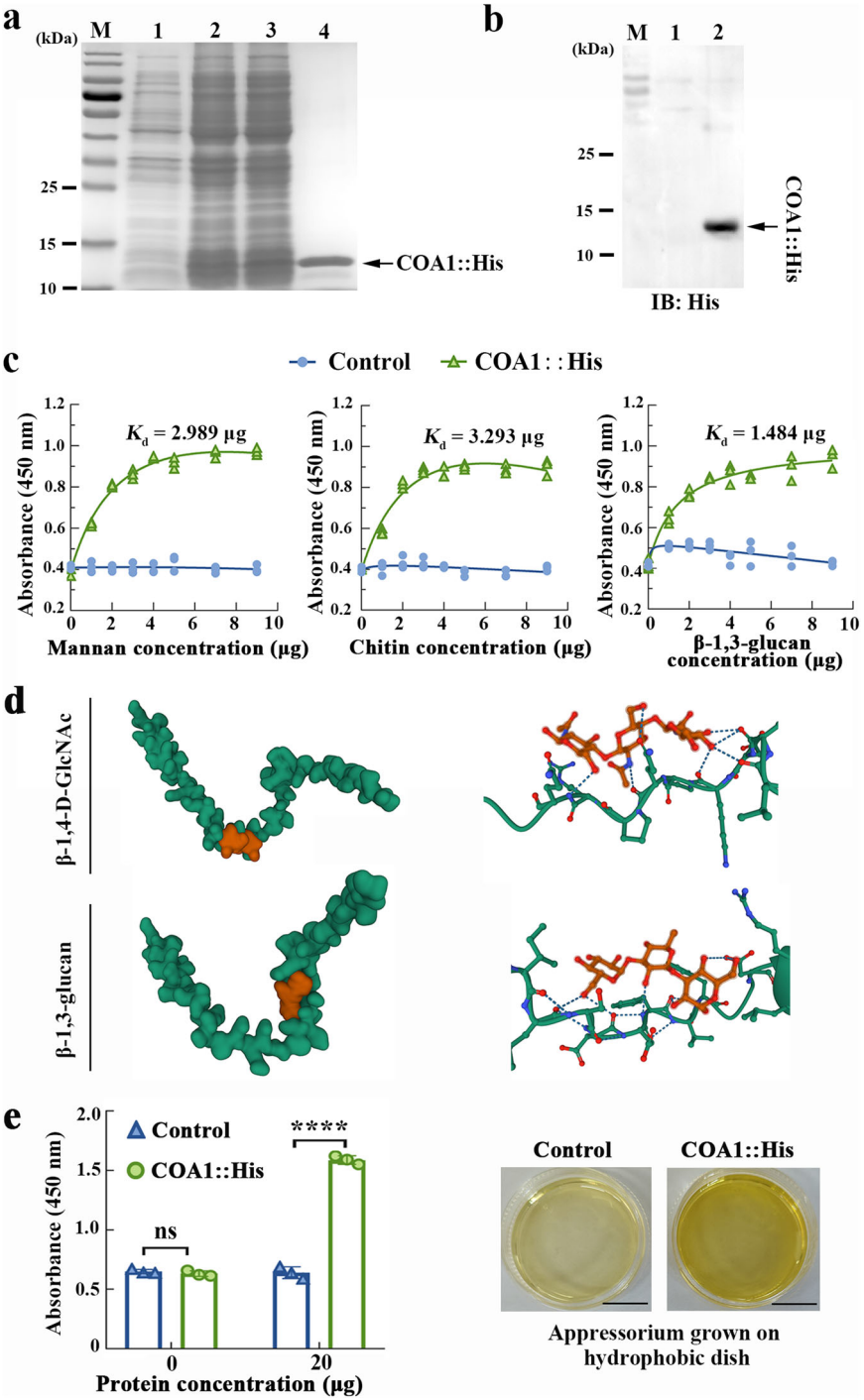

Fig. 4 | Carbohydrates binding assay. Heterologous expression and purification of COA1::His protein. **a** SDS-PAGE. **b** Western blot. M: Protein ladder. 1: Crude extract from *E. coli* with empty vector (pET-28a, control). 2: Crude extract from *E. coli* with pET-28a-Coa1. 3: Supernatant of sample 2. 4: Proteins purified from sample 3 by HisPur Ni-NTA Resin. The black arrow indicates the recombinant COA1::His protein. **c** Binding of COA1 to carbohydrates. Purified proteins (20 μg) were added to mannan, chitin, or β-1,3-glucan at varying concentrations, and the binding values were measured by absorbance at 450 nm. The K_d values were calculated from the binding curves using a one-site binding model in GraphPad Prism. **d** Binding mode of carbohydrates to COA1 by molecular docking. On the left panel, the Molecule of the Month feature is presented as a cartoon illustration of the crystal structure of COA1 and β-1,4-D-GlcNAc (upper) and β-1,3-glucan (lower). The right panel shows interactive hydrogen bonds between COA1 and compounds. COA1 is shown in green, and the ligand is in orange. The blue dashed lines denote interactive hydrogen bonds. **e** The binding of COA1 to fungal cells was examined by incubating 0 or 20 μg of proteins with appressoria generated from conidia inoculated on hydrophobic dishes for 14 h. Representative colorimetric pictures are shown on the right. Scale bar, 1 cm. **** means a significant difference compared to the control ($n = 3$, $P < 0.0001$, two-tailed Student's t test). Data represent the mean ± SD.

decreased after the inoculation of WT or *ΔCoa1* compared to the mock control (Fig. 6d). The calculation of Shannon index of OTU level in WT or *ΔCoa1* was significantly lower than that of the mock control ($P < 0.01$), which means that infection with *M. robertsii* reduced gut microbiota species diversity (Fig. 6e). Principal co-ordinates analysis (PCoA) based on weighted-UniFrac (W-UniFrac) was used to assess bacterial community diversity between samples. According to PCoA results, the first two axes accurately predicted 98.89% and 1.03% of total variability in bacterial communities (Fig. 6f). ANOSIM (analysis of similarities) confirmed that the fungi-treated groups showed a marked difference from the mock-treated group ($R = 0.3333$, $P = 0.008$) (Fig. 6f). Taken together, these results revealed that being infected with *M. robertsii* could reduce gut bacterial species diversity and result in gut microbiome dysbiosis. Besides, the deletion of *Coa1* significantly reduced the gut bacterial load.

Deletion of *Coa1* decreases hemocoel bacterial load

Several studies have shown that infection by entomopathogenic fungi causes bacterial translocation from the gut to the hemolymph. We further examined the effect of fungal infection on bacterial load in the hemocoel. The hemolymph was collected and plated on LB medium for colony counting after topical infection with mock, WT, or *ΔCoa1* for 24, 48, 72, and 96 h. There was no statistical difference between mock, WT, or *ΔCoa1*-infected insects at 24 and 48 h. In the hemolymph of WT-infected insects, the bacterial load peaked at 72 h before declining to the initial level (Fig. 7a).

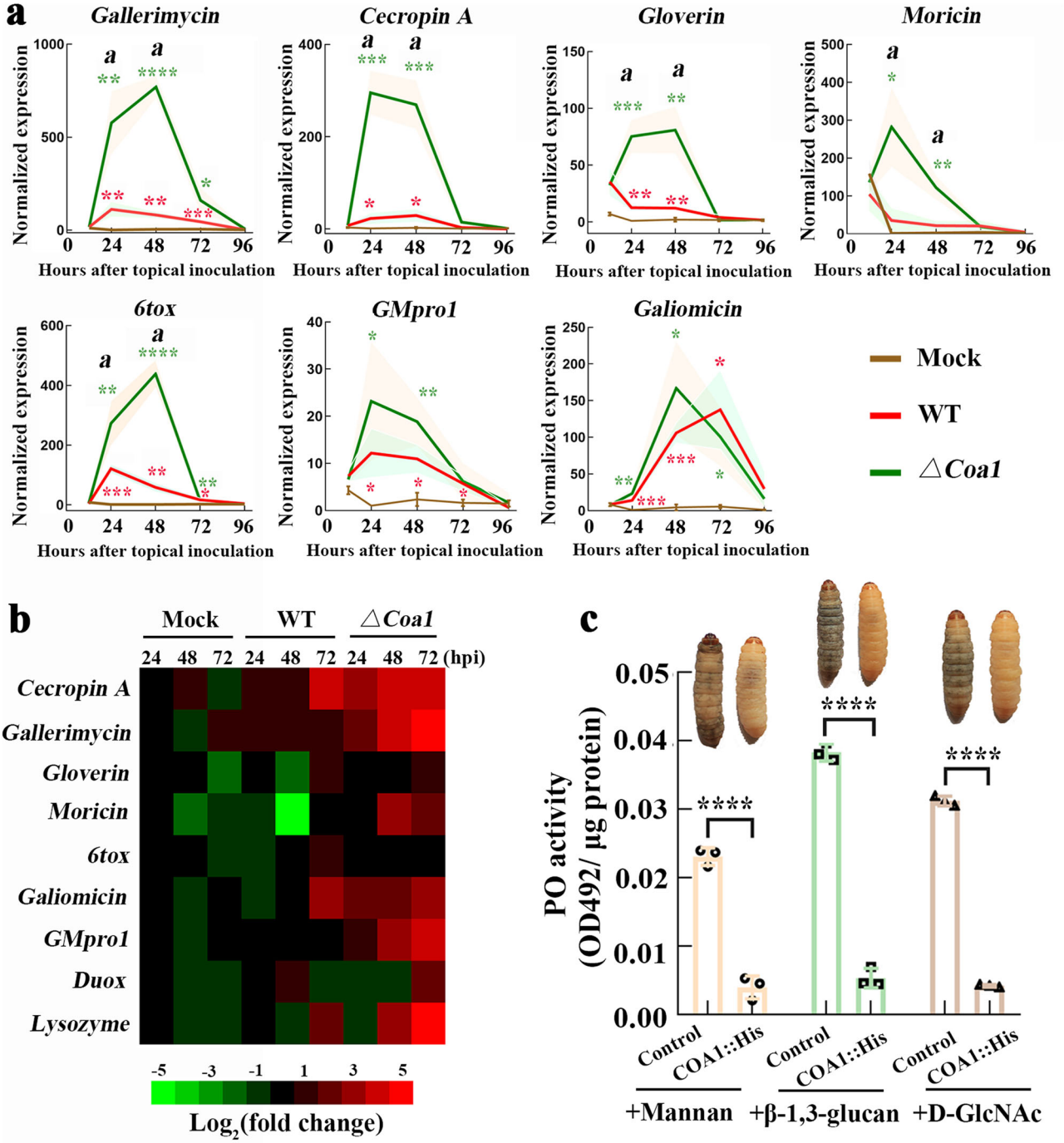

Fig. 5 | Effects of COA1 on the immune escaping. a AMP expression in fat bodies after being topically infected with the WT and *ΔCoa1*. The expression level of each AMP at 24 h in the mock control was set as 1. The plot includes a shade that represents the error bar. The green or red asterisks mean a significant difference in the *ΔCoa1* or WT compared to the mock at each time point, and the letter means a significant difference between WT and *ΔCoa1* at each time point ($n = 3$, $^{*}P < 0.05$, $^{**}P < 0.01$, $^{***}P < 0.001$, $^{****}P < 0.0001$, *a:* $P < 0.05$, two-tailed Student's *t* test). **b** qRT-PCR analysis to assess the immune effectors' expression in the gut following topical infection with various strains. The gene expression at 24 h in the mock is normalized to 1. The values were subjected to log2 transformation. **c** Phenoloxidase activity in the hemolymph after the *G. mellonellla* larvae injected with protein-carbohydrate mixtures for 10 min. Control: Crude extract from *E. coli* containing empty vector pET-28a. Representative pictures of the *G. mellonella* larvae are shown after injection with the mixture of protein and carbohydrates. **** means a significant difference ($n = 3$, $P < 0.0001$, two-tailed Student's *t* test). Data represent the mean ± SD.

Conversely, the bacterial load remained constantly low in the insects infected with the *ΔCoa1* and was significantly lower than WT-infected insects at 72 h ($P < 0.001$) (Fig. 7a). Absolute quantitative PCR was also performed to analyze the total bacterial genomic DNA in the collected hemolymph, which confirmed the same trend as the colony counting (Fig. 7b). There was no significant difference between WT and C-*ΔCoa1* (Fig. 7a, b).

Effect of gut bacteria on fungal virulence

As shown in Fig. 7a, three primary bacterial colony morphotypes were observed in the WT-infected insects' hemocoel. 16S rDNA sequencing was used to determine the selected bacteria. After performing the sequence alignments using the BLASTN analysis of NCBI, the three bacteria were identified as *Enterococcus faecalis* (G positive, G+), *Klebsiella pneumoniae*

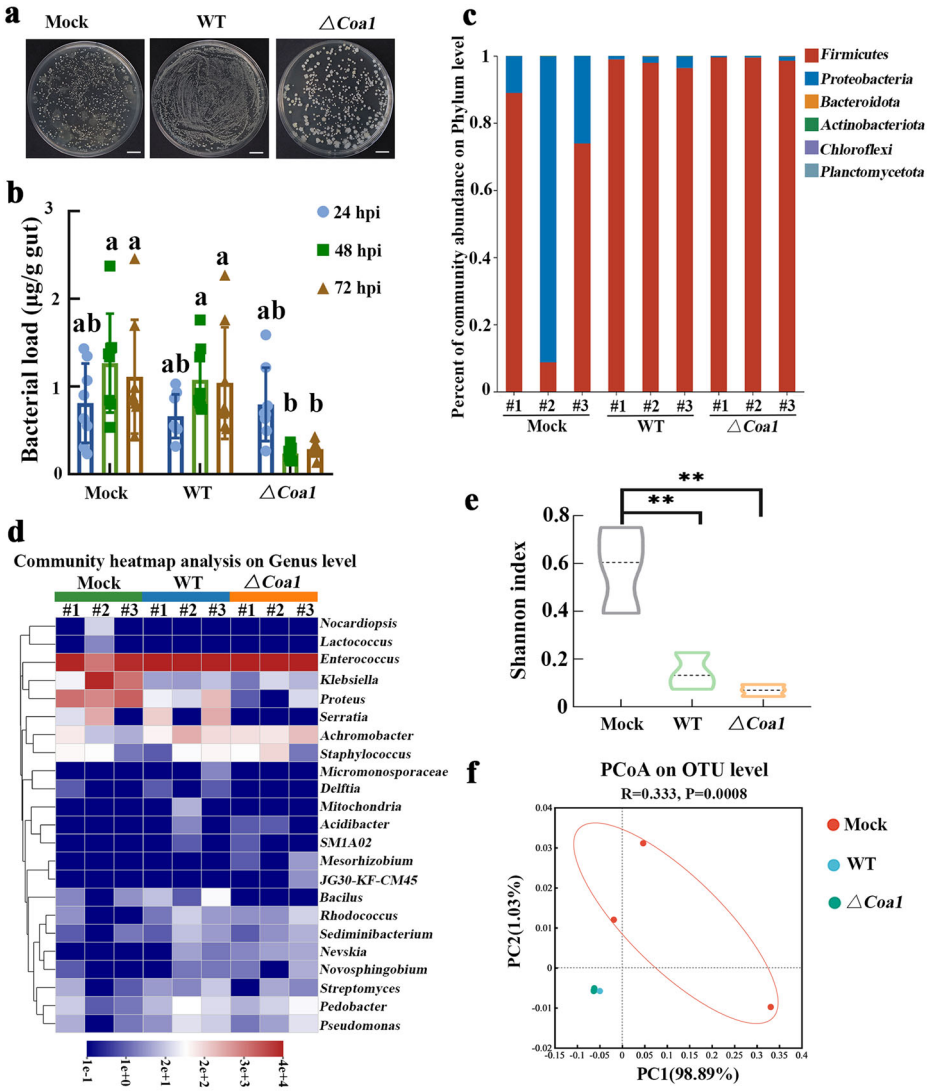

Fig. 6 | Alterations in the insect gut microbiome. **a** CFU formation of the bacteria collected from the insect's gut after topical infection with different strains for 48 h. The LB plates were photographed after 2 days of incubation at 37 °C. Scale bar, 1 cm. **b** Quantitative PCR analysis of the gut bacterial load. Each point represents a single gut. Data represent the mean ± SD. Different letters mean a significant difference ($n = 8$, $P < 0.05$ by Tukey's test in two-way ANOVA). **c** The box plot depicts the relative abundances of the bacterial phyla. **d** Heatmap showing the dynamics of bacterial community at the genus level. **e** Variation in the α-diversity indices of Shannon between treatments. ** means a significant difference ($n = 3$, $P < 0.01$, Tukey's test in one-way ANOVA). **f** Principal co-ordinates analysis (PCoA) based on the weighted-UniFrac (W-UniFrac) showed a separation of bacterial community between fungi and mock treatment.

(G negative, G−), and *Serratia marcescens* (G−), respectively. Injection with *E. faecalis*, *K. pneumoniae*, and *S. marcescens* significantly decreased the survival rate of *G. mellonella* (Fig. 7c).

To further explore the effect of gut microbiota on fungal virulence, we treated *G. mellonella* larvae with gentamicin (30 μg/mL), penicillin (20 units/mL), and streptomycin (20 μg/mL) antibiotics for seven days to obtain the antibiotic-treated larvae, in which gut bacterial load was significantly depleted. Plating and colony counting verified the reduction in gut bacteria (Supplementary Fig. 7). The fungal virulence was examined using both the antibiotic-treated and untreated *G. mellonella* larvae. Via topical infection with either the WT or the C-*ΔCoa1* strains, the survival rate of antibiotic-treated larvae was significantly higher than untreated larvae ($P < 0.01$) (Fig. 7d). There was no significant difference ($P > 0.05$) between the antibiotic-treated and untreated larvae when topical infection with *ΔCoa1*(Fig. 7d). The results suggested that gut bacteria could facilitate the fungal killing of insects.

The toxin destruxin can regulate the AMP expression in *G. mellonella*

As shown in Fig. 5a, AMPs expression level reverted to the baseline after fungal invasion of the insect hemocoel. Previous research indicates that destruxin can suppress the host's cellular immune response and melanization activity[15]. We thus investigate if destruxin could modulate the expression of AMPs. The fat bodies were collected after injecting five microlitres of 200 μM destruxin B into *G. mellonella* larvae. The result showed that all the AMPs except for *galiomicin* were downregulated at 3 h in the destruxin-injected larvae compared to the PBS-injected larvae (Fig. 8a). However, no significant difference was observed between the destruxin and PBS treatments at 12 h ($P > 0.05$, Fig. 8a). To assay the effect of COA1 on destruxin production in the real hemocoel, we constructed *WT-PDtx3-GFP* and *ΔCoa1- PDtx3-GFP* strains following previous methods[19]. GFP fluorescence intensity represented the expression of *Dtx3* (*MAA_10045*). Results revealed no significant difference between the two strains, indicating COA1 did not influence destruxin production (Fig. 8b).

Discussion

The host cellular and humoral immune attack, long believed to occur primarily after pathogenic fungi enter the hemocoel, actually begins earlier. In fact, the insect exoskeleton, often viewed as merely a passive protection layer, actively participates in immune defense[25,32]. This prompts the question of which strategies entomopathogenic fungi take to cope with host immune challenges during cuticle penetration. This study found that the entomopathogenic fungus *M. robertsii* has evolved a coat protein COA1 to evade host immune recognition during cuticular penetration by binding to and masking fungal surface carbohydrates. Deletion of *Coa1* provokes an intense humoral immune response, resulting in a reduction of bacteria in the gut and hemocoel and a decrease in fungal virulence (Fig. 9). To our knowledge, COA1 and its homologs have not been studied before.

Deletion of *Coa1* has little impact on fungal growth but increases sensitivity to high salt stress. Salt stress does not affect the expression of *Coa1*

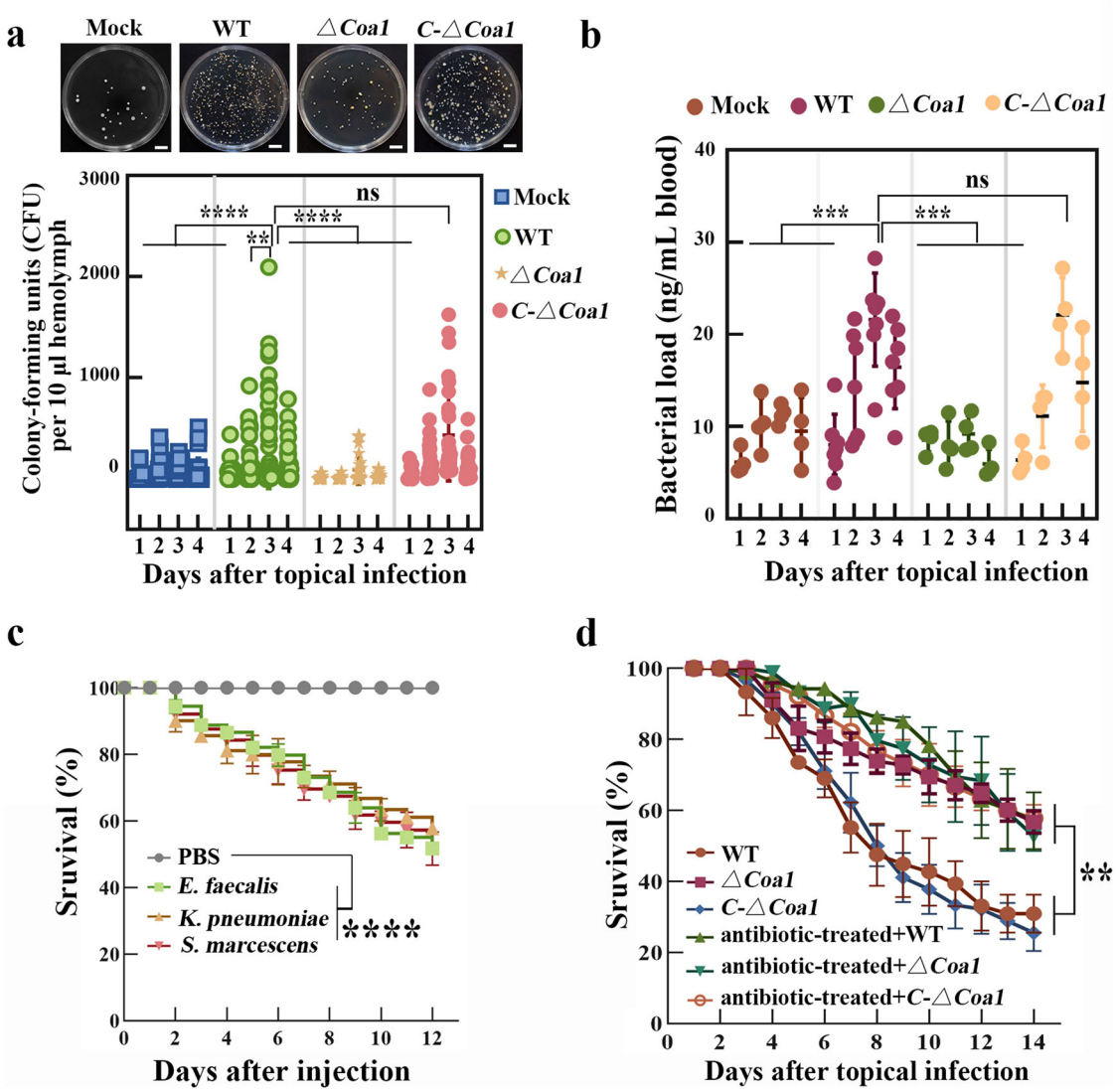

Fig. 7 | Effect of bacteria on fungal pathogenicity. a CFU assay of the bacterial burden collected from the hemolymph. The LB plates were incubated for 48 h at 37 °C. Each point represents an insect. Upper, representative pictures of bacteria in the hemolymph collected from insects after topical infection with different strains for three days. Scale bar, 1 cm. Data represent the mean ± SD. ** ($P < 0.01$) and **** ($P < 0.0001$) mean a significant difference compared to other conditions ($n = 24$–40 insects per condition, Tukey's test in one-way ANOVA). **b** Absolute quantitative PCR analysis of bacterial load in *G. mellonella* hemolymph. Each dot represents a mixture of three insects hemolymph. Data represent the mean ± SD. ***$P < 0.001$, ****$P < 0.0001$, $n = 4$–7, *P*-values were calculated using Tukey's test in one-way ANOVA. **c** Survival curves of *G. mellonella* after being injected with PBS, *E. faecalis*, *K. pneumoniae*, or *S. marcescens*. Five microliters of a bacterial suspension (1×10^5 CFU/mL) were injected into the hemocoel of *G. mellonella* larvae. **d** Survival curves of antibiotic-treated or untreated *G. mellonella* larvae after topical infection with WT, *ΔCoa1* or *C-ΔCoa1*. Experiments were repeated three times with 30 insects per experiment. The asterisks indicate a significant difference (**$P < 0.01$, ****$P < 0.0001$, Tukey's test in one-way ANOVA).

and the function of COA1 in dealing with salt stress warrants further exploration. Under appressorium formation conditions, including simulated conditions and real insect cuticles, expression of *Coa1* is significantly induced to a level similar to the reference gene *actin*, and the COA1 protein is located on the cell wall surface. During cuticle penetration, *Coa1* is directly and positively regulated by the transcription factor COH2, which our previous study confirmed to function in penetrating cuticles via regulation of 44 cuticle-degrading genes[19]. Exploration of COA1 further confirms the essential role of COH2 in fungal pathogenicity and the multi-target characteristic of COH2, suggesting that COH2 may function as a global regulator during cuticle penetration.

The silkworm larva *Bombyx mori* mounts an immunological response and expresses *cecropin* when the cuticle is slightly damaged in the presence of live bacteria or bacterial cell wall components[32]. For cuticular penetration, *M. robertsii* punches a hole in the cuticle with infection structures and cuticle-degrading enzymes. This disruption might trigger immune recognition involving fungi or cuticle-associated bacteria. Moreover, additional cell wall components are exposed during fungal morphogenesis (including conidia germination, hyphal branching, and appressorium formation), potentially proving targets for host immune receptors[13]. Indeed, *G. mellonella* can recognize *M. robertsii* and mount immune responses during cuticle penetration, as observed in this study. Due to the abundant COA1 that can bind to and mask the fungal cell wall carbohydrates, the invading fungi can induce an appropriate immune response in the fat body cells and guts. Deletion of *Coa1* evoked intense immunoreactivity, manifesting as increased AMPs, duox, and lysozyme expression. An absence or overactive immune response is detrimental to insects. John et al.[33] have shown that *G. mellonella* can assess the extent of microbial threat and initiate differential activation of cellular and humoral immune responses. In this study, significantly enhanced PO activity after being injected with carbohydrates demonstrates this point to some degree.

Expression of AMPs in the fat body cells increases at 24 and 48 h but declines at 72 or 96 h. One explanation for this phenomenon might be that the fungal cell wall structure is remodeled to mask the epitopes after entering

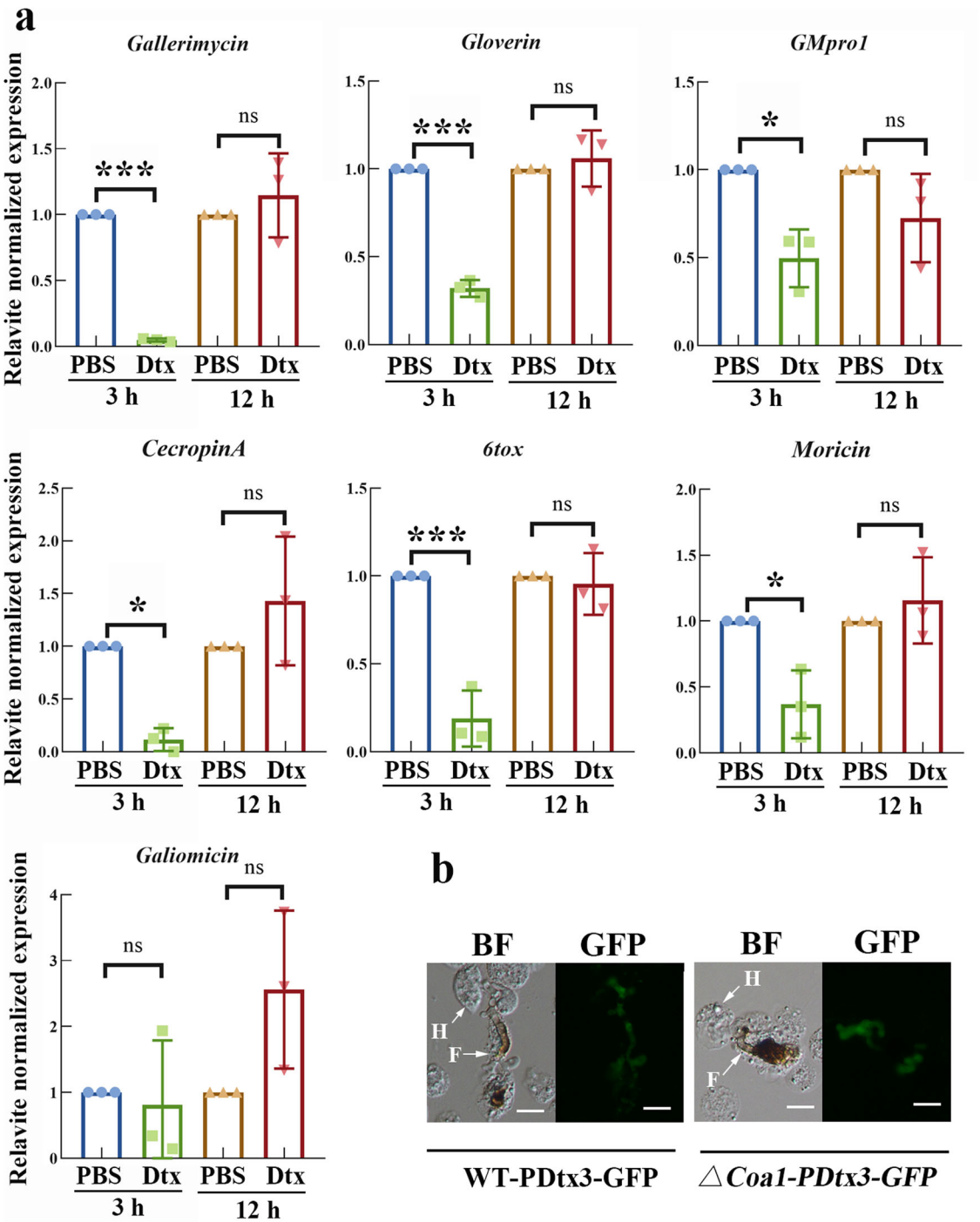

Fig. 8 | Destruxin can regulate the host's immune response. a qRT-PCR analysis of AMPs in fat bodies after injection with five microlitres of 200 μM destruxin B for 3 and 12 h. AMP expression in the fat bodies collected from the PBS-injected larvae was set as 1. Dtx, destruxin B. Data represent the mean ± SD. Asterisks mean a significant difference ($n = 3$, $^{*}P < 0.05$, $^{***}P < 0.001$, two-tailed Student's t test). **b** GFP signal of the fungi in the hemolymph after being injected with different strains for 48 h. BF bright field, F fungal cell, H hemocyte. Scale bar: 10 μm.

the hemocoel[13]. Another explanation could be that the destruxin produced by the fungi after entering the hemocoel suppresses the host's humoral immune response[15,34]. In this study, we demonstrated that destruxin B transiently affects the host immune system, with injection with destruxin B suppressing AMP expression at 3 h but not 12 h. The reason might be that apart from the detoxification process to metabolize the destruxin to other substances[35], the host also secretes the dedicated peptide Baramicin A to inhibit the toxin's effect[36]. A study on *M. rileyi* pathogenesis in the cotton bollworm *Helicoverpa armigera* reveals that after injection with blastospores, the plasma from axenic larvae shows a higher level of plasma antibacterial activity[37]. This suggests that the humoral immune response might respond to the entomopathogenic fungi rather than the bacteria in the hemocoel. This could explain why the AMPs are not upregulated at 72 h after topical infection with *M. robertsii* in this study, even though hemocoel bacterial load increases at this time point.

Several studies have revealed that pathogen infection causes gut microbiota dysbiosis, which damages the peritrophic matrix's (PM) integrity and disrupts the intestinal barrier[26,38–40]. Besides, the entomopathogenic

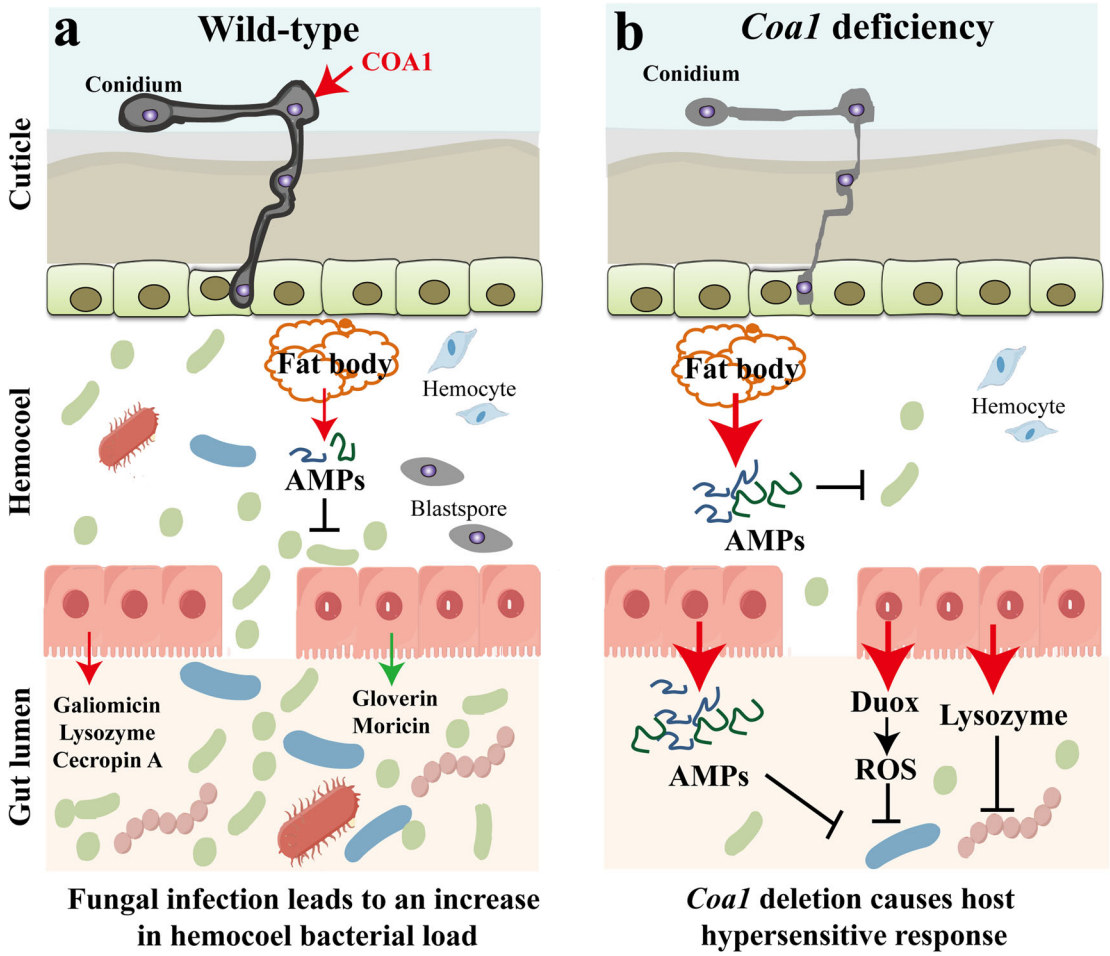

Fig. 9 | Strategic diagram of the interaction between fungi, bacteria, and host during *M. robertsii* penetrating the insect cuticle. a COA1 relocates to the cell surface during cuticle penetration and forms a stealth coating to help fungi evade the host's robust immune responses. Infection with *M. robertsii* perturbs the gut immune AMPs' homeostasis, leading to microbiome dysbiosis and an amplified hemocoel bacterial load. The gut-derived bacteria accelerate the killing speed of fungi. **b** Deletion of *Coa1* provokes a robust immune response, manifesting as the upregulation of AMPs, duox, and lysozyme, which significantly reduces the microbial load. The red arrow indicates upregulation, while the green indicates downregulation. The thickness of the arrows represents the degree of upregulation. This picture was drawn by using Figdraw (www.figdraw.com).

fungus *M. rileyi* also upregulates the chitinase-like protein EN03, which is involved in PM degeneration and thus might contribute to PM impairment[38,41]. Disruption of the barrier can result in the migration of bacteria from the gut into the hemocoel. Indeed, topical infection with *M. robertsii* leads to increased bacteria in the hemocoel at 72 h. Certain symbiotic bacteria, such as *E. faecalis*, migrate from the gut to the hemocoel, transforming into pathogens that can cause host death[42]. After injection with *B. bassiana*, the opportunistic bacterium *S. marcescens* translocates to the hemocoel, accelerating mosquito mortality[26]. In this study, bacterial load in the hemocoel rises at 72 h after topical infection with *M. robertsii*, and three opportunistic pathogens, *S. marcescens*, *E. faecalis*, and *K. pneumoniae*, were found in the hemocoel. The *Coa1* deletion mutant causes an intense immune response, leading to a sharp reduction in intestinal and hemocoel bacterial load, and a slower rate of insect lethality. This reflects the essential role gut bacteria play during the fungal pathogenic process. Consistent with these findings, gut microbiota can accelerate insect mortality after topical infection with *B. bassiana*[26,43]. However, some studies have indicated differing conclusions. For instance, no significant difference in fungal virulence is observed when non-axenic and axenic *H. armigera* were injected with *M. rileyi* blastospores[37]. Moreover, axenic cockroaches had a significantly higher mortality rate than non-axenic cockroaches after oral feeding with *M. anisopliae*[44]. The fungal inoculation methods used (topical infection, injection, or oral feeding), together with the divergent gut microbiota compositions across different insect species, might explain these inconsistent results.

During early infection, *M. robertsii* expresses COA1 to shield cell surface polysaccharides, thereby avoiding the elicitation of robust immune responses and maintaining the hemocoel bacterial load. The microbes in the hemocoel can help accelerate the death of the insect[26,43]. The fungi have to outcompete the bacteria and become predominant in the late stage, as the bacteria compete for nutrients and inhibit fungal growth[37]. Indeed, a substantial reduction in bacterial load is observed after the death of *B. bassiana*-infected insects, due to the synthesis of oosporein[45]. Recently, a study has reported that *M. rileyi* can induce and utilize host AMPs to clear bacteria in the hemocoel before insect death[37]. However, in this study, we traced AMP expression up to 96 h, during which no significant upregulation was observed. The question of whether cellular and humoral immune activity increases, or whether fungi secrete other secondary metabolites to inhibit bacteria in dying and dead insects, remains to be explored.

COA1 homologous proteins can be found in *Metarhizium* species, including *M. anisopliae*, *M. majus*, *M. brunneum*, *M. humberi*, and *M. guizhouense*. However, COA1 is absent in *M. album* and *M. acridum*, which have narrow host ranges. The introduction of COA1 and cuticle-degrading enzymes[46], acquired through horizontal gene transfer into *Metarhizium* species with narrow host ranges might expand their host range and accelerate the insecticidal rate.

In conclusion, we have elucidated the mechanism by which the entomopathogenic fungus uses a secretory small protein to evoke an appropriate immune response and manipulate host microbiota to facilitate infection. During cuticle penetration, evading host immune surveillance is so critical that it impacts the gut and hemocoel microbiome, and fungal virulence. Our results paint a fascinating picture of the immune interplay between insects and fungal pathogens during cuticle penetration, a topic that is just beginning to attract attention.

Methods

Fungal strains

Metarhizium robertsii ARSEF 2575 was cultured on potato dextrose agar (PDA; BD Difco) at 26 °C for 14 days to collect conidia. To evaluate the stress tolerance capacity, 5 μl of conidial suspensions (1×10^7 conidia/mL) were inoculated on PDA supplemented with Congo red (1 mg/mL), Calcofluor white (100 μg/mL), sorbitol (1 M), 0.02% H_2O_2, menadione (0.03 mM) and NaCl (0.7 M) and subsequently incubated at 26 °C for seven days.

Gene deletion and fungal transformation

Gene deletion was conducted via *Agrobacterium tumefaciens* AGL1 mediated transformation as previously described[47]. Briefly, PCR was used to amplify the *Coa1* flanking sequence using genomic DNA as a template, which was then inserted into the master plasmid pPK2-Sur-GFP to transform the wild-type strain[47]. The promoter, ORF, and terminator fragments were amplified and inserted into the plasmid pPK2-Bar-GFP to complement *ΔCoa1*[47]. To investigate the localization of COA1, a cassette containing the GFP gene, fused at the C-terminus of *Coa1* driven by the *Coa1* promoter, was used to transform *ΔCoa1*. The obtained strain was named *ΔCoa1-PCoa1-COA1-GFP*. The strain *ΔCoa1-PCoa1-GFP*, which only expressed GFP, was used as a control. Supplementary Table 2 contains a list of primers utilized for this study.

ChIP-qPCR assay

The ChIP-qPCR assay was conducted as described earlier[19]. In brief, the conidia (1×10^8) of the strain *WT-COH2-FLAG* and *WT-FLAG* (used as control) were cultured in SDY medium for 36 h. The mycelium was collected and cross-linked with 1% formaldehyde (Sigma-Aldrich). After shearing using an M220 (Covaris, Woburn, MA, USA), the FLAG-fusion protein-DNA complex was immunoprecipitated with an anti-FLAG antibody (ABclonal, China). The enriched DNA was purified and used for qRT-PCR. The relative enrichment values were determined by dividing the immunoprecipitated DNA by the input DNA.

Quantitative gene expression analysis

qRT-PCR was used to profile the transcription level of *Coa1* during saprophytic growth, cuticle penetration, and hemocoel colonization (growth in *G. mellonella* hemolymph).

To obtain the mycelium penetrating the cuticle, we inoculated 1×10^6 conidia on the *G. mellonella* cuticle on a water-agar plate. After 30 h of inoculation, the cuticle and fungal cultures were used for RNA extraction. The preparation of RNA samples from insect hemolymph to mimic hemocoel colonization was conducted as described earlier[19]. A total of 1×10^5 conidia were inoculated into 250 μL of *G. mellonella* larvae hemolymph, mixed with an equal volume of anticoagulant solution. After 36 h, the pellet was rinsed with sterile water and collected for RNA extraction. The reference genes were *actin* and *tef*[48]. The normalized expression of genes was calculated using the $2^{-\Delta\Delta Ct}$ method[49].

Pathogenicity assays

The virulence of WT and *ΔCoa1* was tested on the last instar *G. mellonella* larvae. Conidia harvested from 14-day-old PDA plates were suspended in 0.01% Triton X-100. Larvae were immersed in 15 ml of spore suspensions (1×10^7 spores/mL) for 15 s for topical infection. An injection to bypass the cuticle was performed by injecting 5 μl of conidia suspension (5×10^4 spores/mL) into the insect hemocoel. The LT_{50} was used to compare the virulence among strains. All tests were performed three times, with 40 insects used for each biological replicate.

As previously stated, the appressorium formation rate was measured on the hydrophobic Petri dish (Corning, NY, USA)[50]. After a 14-h induction, the lipid droplets in the appressoria were measured using Bodipy dye 493/503 (Amgicam, China).

As previously described, the ability to penetrate insect cuticles was assessed[19]. A total of 2 μl of spore suspensions (1×10^7 spores/mL) were inoculated onto the *G. mellonella* cuticle placed on PDA plates supplemented with ampicillin and kanamycin. After two days of inoculation at 26 °C, the cuticle was removed and the fungi were allowed to grow for an additional two days. The colony diameter indicated the cuticle penetration ability. Three biological replicates were performed.

Assays of immune effectors expression and phenoloxidase activity

The genes encoding AMPs included *gallerimycin* (GenBank: AF453824.1), *galiomicin* (GenBank: AY528421.1), *G. mellonella proline-rich protein* (GMpro1, accession number: FJ494919.1), *gloverin* (GenBank: AF394588.1), *moricin* (accession number: EF564366.1), *6tox* (GenBank: AF394584.1), and *cecropin A* (accession number: XM_052900821.1). The accession numbers for *duox* and *lysozyme* are XM_052897526.1 and XM_026899456.3 respectively. Five insects were dissected at each time point after topical infection with different strains for 30 s to obtain fat bodies or gut for total RNA extraction. The 18S rRNA gene of *G. mellonella* (GeneBank number: AF286298) was utilized as the reference gene.

For phenoloxidase activity analysis, hemolymph from five insects was mixed with PBS buffer, and the BCA Kit (Meilunbio, China) was used to determine the total protein content. Hemolymph (50 μg of protein per sample) was mixed with 5 mM $CaCl_2$ solution to a volume of 20 μl before being mixed with 80 μl of 10 mM L-DOPA (pH 6.6). The absorbance was measured at 492 nm after being incubated for 30 minutes at 26 °C. Hemolymph collected from uninoculated insects was used as the mock control. Phenoloxidase (PO) activity was expressed as the OD492 per μg of protein.

Localization analysis of COA1

To investigate the localization of COA1, a strain expressing COA1::GFP fusion protein was constructed. A strain expressing GFP was used as the control. Appressoria were obtained by culturing conidia on a hydrophobic Petri dish containing 0.0125% yeast extract for 16 h. The fungal cell wall was labeled with the chitin-binding fluorescent dye Calcofluor white (CFW, MKBio, China). Twenty larvae were immersed in 15 ml of fungal conidia suspensions (1×10^7 spores/mL) for 30 s. After 48 h, insects were frozen in a −80 °C refrigerator, and cuticles were dissected to observe the localization of COA1 on the *G. mellonella* cuticle.

Cell wall polysaccharide staining

To evaluate the exposure of cell wall polysaccharides, fungal germlings and appressoria were stained with various fluorescent lectins and β-1,3-glucan antibodies. Alexa Fluor 488-labeled lectins ConA (for detecting mannan), HPA (for detecting α-N-Acetylgalactosamine residues), PNA (for detecting terminal β-galactose), and WGA (for detecting chitin) were purchased from Thermo Fisher Scientific, and dissolved in suitable buffers[13]. After washing with PBS, samples were stained with lectins in the dark for 1 h. For detection of β-1,3-glucan, samples were incubated with the anti-β-1,3-glucan antibody (Abcam, ab233743; dilution 1:500) overnight and then with a FITC-conjugated secondary antibody (ABclonal, China; dilution 1:200) as previously described[50]. The samples were imaged using fluorescence microscopy (Nikon, Ni-E), and Image J software (https://imagej.nih.gov/ij) was used to calculate fluorescence intensity.

Binding of COA1 to carbohydrates

As previously stated, COA1 and carbohydrate-binding assays were carried out[51]. In brief, each well of a 96-well plate was coated with different

concentrations of β-1,3-glucan (Yuanye, China), mannan (Yuanye, China), or chitin (Solarbio, China) overnight at room temperature. For the analysis of COA1 binding to fungal cells, 2×10^6 conidia were inoculated into 3 mL of 0.0125% yeast extract in 35 mm hydrophobic dishes. Following inoculation at 26 °C for 14 h, the appressoria were prepared for the binding assay. After blocking with 1 mg/ml BSA in Tris buffer for 2 h at room temperature and washing with Tris buffer, the wells or the dishes were incubated with 20 μg per well of a crude extract of *E. Coli* containing either an empty vector pET-28a or COA1::His protein in the presence of 0.1 mg/ml BSA for 3 h at 26 °C. The plates were then washed four times with Tris buffer, and all subsequent washes followed this procedure. After incubation with an anti-His antibody (ImmunoWay Biotechnology; dilution, 1:1000) overnight at 4 °C and peroxidase-conjugated goat anti-mouse IgG (ABclonal, China; dilution, 1:3000) for 2 h at 26 °C, the plates were treated with 100 μl of TMB (Beyotime Biotechnology, China) for 10 min, followed by termination with 100 μl of 2 M H_2SO_4. The absorbance at 450 nm was then measured using a microplate reader (BioTek, Synergy Neo2).

Molecular docking

The binding affinities between carbohydrates and COA1 were explored using AutodockVina 1.2.2[52]. The molecular structure of COA1 was predicted by SWISS-MODEL (https://swissmodel.expasy.org/). The 3D structures of β-1,3-glucan trimer (PubChem CID, 439306) and GlcNAcbeta1-4GlcNAcbeta1-4GlcNAcbeta (PubChem CID, 444514) were downloaded from PubChem (https://pubchem.ncbi.nlm.nih.gov/). For the docking analysis, all protein and molecular files were converted to PDBQT format, polar hydrogen atoms were added, and water molecules were removed. The grid box was positioned centrally to allow unrestricted molecular mobility and cover each protein's domain. The grid point distance was set at 0.05 nm, and the dimensions of the grid box were 30 Å × 30 Å × 30 Å.

Cell wall contents measurement

Fungal conidia (10^8) were cultured in 100 mL of PDB for 36 h at 26 °C to collect mycelia for cell wall content analysis. The chitin concentration was tested using a chitin ELISA kit (YaJi Biological, China), following the manufacturer's instructions.

The mannan content was quantified using the Alcian Blue method, as previously outlined[53], with slight adjustments. Specifically, 200 mg of mycelia were resuspended in 1 mL of Alcian Blue (MedChemExpress, China) at a concentration of 50 μg/mL in 0.02 M HCl, pH 3.0. The mycelia were centrifugated at 12,000 rpm to pellet after a 10-minute incubation at 26 °C. The absorbance of the supernatants at 600 nm was then measured. The binding of Alcian Blue to the fungal mycelium was measured by subtracting the OD600 of the supernatants from that of the initial solution. A standard curve was established using different concentrations of Alcian Blue.

The quantity of β-1,3-glucan was quantified utilizing the aniline blue assay[54]. A total of six milligrams of lyophilized mycelium were reconstituted in 1 mL of 1 M NaOH and subjected to sonication for 1 min, followed by incubation at 52°C for 30 minutes. Subsequently, 50 μL of supernatants were combined with 150 μL of a working solution containing 0.067% (wt/vol) aniline blue. After incubating for 30 min at 52 °C and an additional 30 min at 26 °C, fluorescence measurements were taken using a fluorescence microplate reader set with excitation/emission wavelengths at 405/460 nm (BioTek, Synergy Neo2). The amount of β-1,3-glucan was represented as fluorescence units.

Gut microbiome analysis

Briefly, 40 insects were immersed in 15 mL of spore suspensions (1×10^7 spores/mL in 0.01% Triton X-100) for 30 s. Mock controls were insects treated with 0.01% Triton X-100. After two days of treatments, five insects per group (consisting of three independent groups in total) were dissected to obtain the guts, which were then used for the gut microbiome analysis. The sequencing analyses were performed by the Majorbio Company (Shanghai, China). Following bacterial DNA lysis, 10 ng of DNA per sample was utilized for amplification with the primers 338 F/806 R (Supplementary Table 2). After a quality check, the PCR products were sequenced on the Illumina HiSeq platform. Normalized sequencing reads were analyzed with Uparse ver.7.0.109 (http://drive5.com/uparse/) to estimate OTUs with a 97% identity cutoff. The α-diversity index, Shannon, was computed based on the discovered OTUs using the tool Mothur.

Hemocoel and gut bacterial load analysis

Larvae were collected, sterilized with 75% ethanol, and bled as described after topical infection with different strains for 24, 48, 72, and 96 h[55]. Ten microliters of hemolymph from each larva were combined with 10 μL of anticoagulant solution and 50 μL of PBS, and then applied onto an LB plate. After two days of incubation at 37 °C, the colony-forming units (CFU) were assessed.

Absolute quantitative PCR (qPCR) was also used to measure the bacterial load by quantifying the bacterial genomic DNA. The genomic DNA of *E. coli* was extracted and a gradient dilution was prepared to use as a template for qPCR, in order to construct a standard curve. To extract DNA from hemolymph, the obtained hemolymph was combined with anticoagulant and centrifugated at 10,000 × *g* for 10 min to obtain precipitates. The guts were dissected, immersed in 1 mL of sterile PBS, and vortexed for 2 min. The supernatant was collected and centrifuged at 10,000 × *g* for 10 min to obtain the precipitates. Total DNA in the hemolymph or gut-derived precipitates was extracted using a genomic DNA extraction kit (Beyotime, China) and used as the template for qPCR. Each time point had at least 8 replicates, with each larva being regarded as a repeat.

Antibiotic treatment of *G. mellonella* larvae

G. mellonella larvae were raised at 24 °C, 70% humidity, and a light/dark cycle of 12 h. The larvae were fed an artificial diet mainly consisting of flour and milk (Keyun Biological Pesticide Ltd. China) until reaching a weight of 200–300 mg. Antibiotic-treated larvae were obtained by oral feeding an artificial diet supplemented with gentamicin (30 μg/mL), penicillin (20 units/mL), and streptomycin (20 μg/mL) for seven days, as described[37].

Statistics and reproducibility

The statistical analyses were conducted using GraphPad Prism 8.2 software. Detailed information regarding the specific statistical methods and parameters employed is provided in the figure legends.

Reporting summary

Further information on research design is available in the Nature Portfolio Reporting Summary linked to this article.

Data availability

The raw data of the gut microbiome was uploaded to the NCBI database (number: PRJNA1050837). All original data underlying the graphs have been included in the Supplementary Data 1 file. Uncropped blot and gel images are shown in Supplementary Fig. 8.

Received: 23 March 2024; Accepted: 3 September 2024;
Published online: 30 September 2024

References

1. Xiao, G. et al. Genomic perspectives on the evolution of fungal entomopathogenicity in *Beauveria bassiana*. *Sci. Rep.* **2**, 483 (2012).
2. St. Leger, R. J., Wang, C. & Fang, W. New perspectives on insect pathogens. *Fungal Biol. Rev.* **25**, 84–88 (2011).
3. Wang, C. & Feng, M.-G. Advances in fundamental and applied studies in China of fungal biocontrol agents for use against arthropod pests. *Biol. Control* **68**, 129–135 (2014).
4. Wang, C. & Wang, S. Insect Pathogenic Fungi: Genomics, Molecular Interactions, and Genetic Improvements. *Annu. Rev. Entomol.* **62**, 73–90 (2017).

5. Pedrini, N., Ortiz-Urquiza, A., Huarte-Bonnet, C., Zhang, S. & Keyhani, N. O. Targeting of insect epicuticular lipids by the entomopathogenic fungus *Beauveria bassiana*: hydrocarbon oxidation within the context of a host-pathogen interaction. *Front. Microbiol.* **4**, 24 (2013).
6. Pedrini, N., Zhang, S., Juárez, M. P. & Keyhani, N. O. Molecular characterization and expression analysis of a suite of cytochrome P450 enzymes implicated in insect hydrocarbon degradation in the entomopathogenic fungus *Beauveria bassiana*. *Microbiology* **156**, 2549–2557 (2010).
7. Beys da Silva, W. O., Santi, L., Schrank, A. & Vainstein, M. H. *Metarhizium anisopliae* lipolytic activity plays a pivotal role in Rhipicephalus (Boophilus) microplus infection. *Fungal Biol.* **114**, 10–15 (2010).
8. Zhang, S. et al. CYP52X1, representing new cytochrome P450 subfamily, displays fatty acid hydroxylase activity and contributes to virulence and growth on insect cuticular substrates in entomopathogenic fungus *Beauveria bassiana*. *J. Biol. Chem.* **287**, 13477–13486 (2012).
9. Sun, Y., Hong, S., Chen, H., Yin, Y. & Wang, C. Production of Helvolic Acid in Metarhizium Contributes to Fungal Infection of Insects by Bacteriostatic Inhibition of the Host Cuticular Microbiomes. *Microbiol. Spectr.* **10**, e0262022 (2022).
10. Hong, S., Sun, Y., Chen, H. & Wang, C. Suppression of the insect cuticular microbiomes by a fungal defensin to facilitate parasite infection. *ISME J.* **17**, 1–11 (2023).
11. Hoffmann, J. A. The immune response of Drosophila. *Nature* **426**, 33–38 (2003).
12. Lemaitre, B. & Hoffmann, J. The host defense of *Drosophila melanogaster*. *Annu Rev. Immunol.* **25**, 697–743 (2007).
13. Wanchoo, A., Lewis, M. W. & Keyhani, N. O. Lectin mapping reveals stage-specific display of surface carbohydrates in in vitro and haemolymph-derived cells of the entomopathogenic fungus *Beauveria bassiana*. *Microbiology* **155**, 3121–3133 (2009).
14. Wang, C. & St Leger, R. J. A collagenous protective coat enables *Metarhizium anisopliae* to evade insect immune responses. *Proc. Natl Acad. Sci. USA* **103**, 6647–6652 (2006).
15. Wang, B., Kang, Q., Lu, Y., Bai, L. & Wang, C. Unveiling the biosynthetic puzzle of destruxins in Metarhizium species. *Proc. Natl Acad. Sci. USA* **109**, 1287–1292 (2012).
16. Feng, P., Shang, Y., Cen, K. & Wang, C. Fungal biosynthesis of the bibenzoquinone oosporein to evade insect immunity. *Proc. Natl Acad. Sci. USA* **112**, 11365–11370 (2015).
17. St Leger, R., Joshi, L., Bidochka, M. J. & Roberts, D. W. Construction of an improved mycoinsecticide overexpressing a toxic protease. *Proc. Natl Acad. Sci. USA* **93**, 6349–6354 (1996).
18. Wang, C., Hu, G. & St Leger, R. J. Differential gene expression by *Metarhizium anisopliae* growing in root exudate and host (*Manduca sexta*) cuticle or hemolymph reveals mechanisms of physiological adaptation. *Fungal Genet. Biol.* **42**, 704–718 (2005).
19. Zhang, X., Meng, Y., Huang, Y., Zhang, D. & Fang, W. A novel cascade allows *Metarhizium robertsii* to distinguish cuticle and hemocoel microenvironments during infection of insects. *PLoS Biol.* **19**, e3001360 (2021).
20. Lu, Z. et al. Multifunctional role of a fungal pathogen-secreted laccase 2 in evasion of insect immune defense. *Environ. Microbiol.* **23**, 1256–1274 (2021).
21. Wang, H. et al. Insect fungal pathogens secrete a cell wall-associated glucanase that acts to help avoid recognition by the host immune system. *PLoS Pathog.* **19**, e1011578 (2023).
22. Gow, N. A. R., Latge, J. P. & Munro, C. A. The Fungal Cell Wall: Structure, Biosynthesis, and Function. *Microbiology spectrum* **5**, https://doi.org/10.1128/microbiolspec.FUNK-0035-2016 (2017).
23. Gottar, M. et al. Dual detection of fungal infections in Drosophila via recognition of glucans and sensing of virulence factors. *Cell* **127**, 1425–1437 (2006).
24. Brown, G. D. & Gordon, S. Fungal beta-glucans and mammalian immunity. *Immunity* **19**, 311–315 (2003).
25. Zheng, X., Li, S., Si, Y., Hu, J. & Xia, Y. Locust can detect β-1, 3-glucan of the fungal pathogen before penetration and defend infection via the Toll signaling pathway. *Dev. Comp. Immunol.* **106**, 103636 (2020).
26. Wei, G. et al. Insect pathogenic fungus interacts with the gut microbiota to accelerate mosquito mortality. *Proc. Natl Acad. Sci. USA* **114**, 5994–5999 (2017).
27. Mesquita, E. et al. Entomopathogenic fungus treatment changes the gut bacterial diversity of Rhipicephalus microplus ticks. *Parasites Vectors* **16**, 185 (2023).
28. Latgé, J. P. Tasting the fungal cell wall. *Cell. Microbiol.* **12**, 863–872 (2010).
29. Masuoka, J. Surface glycans of *Candida albicans* and other pathogenic fungi: physiological roles, clinical uses, and experimental challenges. *Clin. Microbiol. Rev.* **17**, 281–310 (2004).
30. Brown, S. E., Howard, A., Kasprzak, A. B., Gordon, K. H. & East, P. D. A peptidomics study reveals the impressive antimicrobial peptide arsenal of the wax moth *Galleria mellonella*. *Insect. Biochem. Mol. Biol.* **39**, 792–800 (2009).
31. Marra, A., Hanson, M. A., Kondo, S., Erkosar, B. & Lemaitre, B. Drosophila Antimicrobial Peptides and Lysozymes Regulate Gut Microbiota Composition and Abundance. *mBio* **12**, e0082421 (2021).
32. Brey, P. T. et al. Role of the integument in insect immunity: epicuticular abrasion and induction of cecropin synthesis in cuticular epithelial cells. *Proc. Natl Acad. Sci. USA* **90**, 6275–6279 (1993).
33. Fallon, J. P., Troy, N. & Kavanagh, K. Pre-exposure of *Galleria mellonella* larvae to different doses of *Aspergillus fumigatus* conidia causes differential activation of cellular and humoral immune responses. *Virulence* **2**, 413–421 (2011).
34. Pal, S., St Leger, R. J. & Wu, L. P. Fungal peptide Destruxin A plays a specific role in suppressing the innate immune response in *Drosophila melanogaster*. *J. Biol. Chem.* **282**, 8969–8977 (2007).
35. Cherton, J. C. et al. Direct in vitro and in vivo monitoring of destruxins metabolism in insects using internal surface reversed-phase high-performance liquid chromatography. I. Behaviour of E destruxin in locusts. *J. Chromatogr.* **566**, 511–524 (1991).
36. Huang, J. et al. A Toll pathway effector protects Drosophila specifically from distinct toxins secreted by a fungus or a bacterium. *Proc. Natl Acad. Sci. USA* **120**, e2205140120 (2023).
37. Wang, J. L. et al. An entomopathogenic fungus exploits its host humoral antibacterial immunity to minimize bacterial competition in the hemolymph. *Microbiome* **11**, 116 (2023).
38. Abraham, N. M. et al. Pathogen-mediated manipulation of arthropod microbiota to promote infection. *Proc. Natl Acad. Sci. USA* **114**, E781–E790 (2017).
39. Zhang, S., Huang, J., Wang, Q., You, M. & Xia, X. Changes in the Host Gut Microbiota during Parasitization by Parasitic Wasp Cotesia vestalis. *Insects* **13**, https://doi.org/10.3390/insects13090760 (2022).
40. Wu, P. et al. A Gut Commensal Bacterium Promotes Mosquito Permissiveness to Arboviruses. *Cell Host Microbe* **25**, 101–112.e105 (2019).
41. Liu, X. et al. Progress and prospects of arthropod chitin pathways and structures as targets for pest management. *Pestic. Biochem. Physiol.* **161**, 33–46 (2019).
42. Mason, K. L. et al. From commensal to pathogen: translocation of *Enterococcus faecalis* from the midgut to the hemocoel of *Manduca sexta*. *mBio* **2**, e00065–00011 (2011).
43. Xu, L. et al. Gut microbiota in an invasive bark beetle infected by a pathogenic fungus accelerates beetle mortality. *J. Pest Sci.* **92**, 343–351 (2018).
44. Zhang, F. et al. The interactions between gut microbiota and entomopathogenic fungi: a potential approach for biological control of Blattella germanica (L.). *Pest Manag. Sci.* **74**, 438–447 (2018).

45. Fan, Y. et al. Regulatory cascade and biological activity of *Beauveria bassiana* oosporein that limits bacterial growth after host death. *Proc. Natl Acad. Sci. USA* **114**, E1578–E1586 (2017).
46. Zhang, Q. et al. Horizontal gene transfer allowed the emergence of broad host range entomopathogens. *Proc. Natl Acad. Sci. USA* **116**, 7982–7989 (2019).
47. Xu, C. et al. A high-throughput gene disruption methodology for the entomopathogenic fungus *Metarhizium robertsii*. *PloS one* **9**, e107657 (2014).
48. Fang, W. & Bidochka, M. J. Expression of genes involved in germination, conidiogenesis and pathogenesis in *Metarhizium anisopliae* using quantitative real-time RT-PCR. *Mycological Res.* **110**, 1165–1171 (2006).
49. Livak, K. J. & Schmittgen, T. D. Analysis of relative gene expression data using real-time quantitative PCR and the 2(-Delta Delta C(T)) Method. *Methods* **25**, 402–408 (2001).
50. Guo, N. et al. Alternative transcription start site selection in Mr-OPY2 controls lifestyle transitions in the fungus *Metarhizium robertsii*. *Nat. Commun.* **8**, 1565 (2017).
51. Yu, X. Q. & Kanost, M. R. Immulectin-2, a lipopolysaccharide-specific lectin from an insect, *Manduca sexta*, is induced in response to gram-negative bacteria. *J. Biol. Chem.* **275**, 37373–37381 (2000).
52. Morris, G. M., Huey, R. & Olson, A. J. Using AutoDock for ligand-receptor docking. *Curr. Protoc. Bioinformatics* Chapter 8, Unit 8.14, https://doi.org/10.1002/0471250953.bi0814s24 (2008).
53. Odani, T., Shimma, Y., Tanaka, A. & Jigami, Y. Cloning and analysis of the MNN4 gene required for phosphorylation of N-linked oligosaccharides in *Saccharomyces cerevisiae*. *Glycobiology* **6**, 805–810 (1996).
54. Fortwendel, J. R. et al. Differential effects of inhibiting chitin and 1,3-{beta}-D-glucan synthesis in ras and calcineurin mutants of *Aspergillus fumigatus*. *Antimicrobial Agents Chemother.* **53**, 476–482 (2009).
55. Zhao, H. et al. Host-to-pathogen gene transfer facilitated infection of insects by a pathogenic fungus. *PLoS Pathog.* **10**, e1004009 (2014).

Acknowledgements

This study was supported by the National Natural Science Foundation of China (32200166). X.H. is supported by the Young Taishan Scholars Program (NO. tsqn202103130).

Author contributions

Q.Z. designed and conducted experiments, drew the figures, and wrote the original draft. X.W. carried out the experiments and drew the figures. W.F. provided constructive comments. X.H. took the images shown in Fig. 2 and polished the language of the manuscript. X.Z. conceived the idea, designed the study, supervised the study, and wrote the paper.

Competing interests

The authors declare no competing interests.

Additional information

Supplementary information The online version contains supplementary material available at https://doi.org/10.1038/s42003-024-06827-w.

Correspondence and requests for materials should be addressed to Xing Zhang.

Peer review information *Communications Biology* thanks the anonymous reviewers for their contribution to the peer review of this work. Primary Handling Editors: Koon Ho Wong and Tobias Goris. A peer review file is available.